J. Phys. E: Sci. Instrum. 19 (1986). Printed in Great Britain

3

CONTRIBUTED PAPERS

Experimental test of a prototype gravitational radiation detector employing an active cavity laser sensor

Alex Abramovici†, Zeev Vager† and Meir Weksler‡
† Department of Nuclear Physics, Weizmann Institute of Science, Rehovot, Israel
‡ Israel Electro Optical Industries, Rehovot, Israel

Received 20 December 1984, in final form 12 June 1985

Abstract. A prototype gravitational radiation detector which uses two small He–Ne lasers in a heterodyne arrangement for displacement sensing has been built and tested. Operation of the system at the theoretical noise limit determined by spontaneous emission has been achieved. Above 2 kHz, the noise has a flat spectrum and is equivalent to displacements of 3×10^{-15} cm Hz$^{-1/2}$.

It is shown that small active-cavity systems can be competitive with long-baseline Michelson interferometers when the high-quality mirrors and high-gain amplifying media now available are used.

1. Introduction

A sizable part of the worldwide effort to detect gravitational radiation (GR) pulses generated by violent cosmic events is devoted to the building of broad-band devices. These rely on test masses which are virtually free in the frequency band of interest between 500 and 10 000 Hz. A laser beam is repeatedly bounced off mirrors attached to the masses so that any change in distance between the masses is seen as a change in parameters of the probing electromagnetic field. An early detector of this type (Forward 1978) consisted of a Michelson interferometer illuminated by a He–Ne laser emitting the 632.8 nm line. All wide-band GR detectors currently under construction are also of the Michelson interferometer type, with either optical delay lines (Billing *et al* 1979, Winkler 1983, Schilling *et al* 1984, Weiss 1972, Linsay *et al* 1983) or optical cavities (Drever 1982) built into their arms in order to increase sensitivity. The interferometers are passive optical systems, since light is fed from an external source, usually an argon ion laser.

For several years now an effort has been under way at the Weizmann Institute to build an active-cavity GR detector, in which the mirrors attached to the test masses define a laser resonator so that a change in mass spacing induces a change in the frequency of the laser field. An early prototype monitored the changes in the beat frequency between two appropriately selected modes of a three-cavity He–Ne laser (Weksler *et al* 1980a, b). The scheme that has been finally adopted relies on monitoring changes in the beat frequency that is obtained by heterodyning two independent lasers. In theory, the sensitivity of such systems is limited by spontaneous emission noise. The system described in the present paper employs two small He–Ne lasers and has been built specifically to check that operation limited by spontaneous emission noise can be achieved. With this system we have measured a noise equivalent displacement of 3×10^{-15} cm Hz$^{-1/2}$, which is, indeed, very close to the expected theoretical limit. A displacement sensor based on two heterodyned lasers has been proposed independently by a Soviet group (Bagayev *et al* 1981).

The description of our system is presented in § 2. Section 3 contains the noise analysis for the active-cavity GR detector. Section 4 describes the expected and measured sensitivity of our prototype detector, which are found to agree closely with each other. We then present an estimate of the minimum energy flux of a GR event detectable with this system. It is shown in § 5 that the sensitivity may be increased by three orders of magnitude by using a high-gain amplifying medium and better mirrors, making the small active-cavity detector a viable alternative to large interferometers developed by other groups. Practical merits of short active-cavity GR detectors are then discussed. Our conclusions are summarised in § 6.

2. Description of the GR detector

2.1. The active-cavity GR antenna

The displacement sensor of our GR detector consists of two similar $\lambda = 632.8$ nm He–Ne lasers, operated in a heterodyne scheme, as shown in figure 1. The laser beams, of frequencies ω_1 and ω_2, combine at the beam splitter and provide, after photodetection, a beat signal of frequency $\omega_B = \omega_2 - \omega_1$. A servo-system maintains ω_B at approximately $2\pi \times 20$ MHz. When the mirror spacings in the two lasers change by ΔL_2 and ΔL_1, respectively, the beat frequency changes by an amount

$$\Delta\omega_B = \omega \frac{\Delta L_2 - \Delta L_1}{L} \tag{1}$$

where ω is the mean value of ω_1, ω_2, and L is the mean value of L_1, L_2, the optical lengths of the laser resonators.

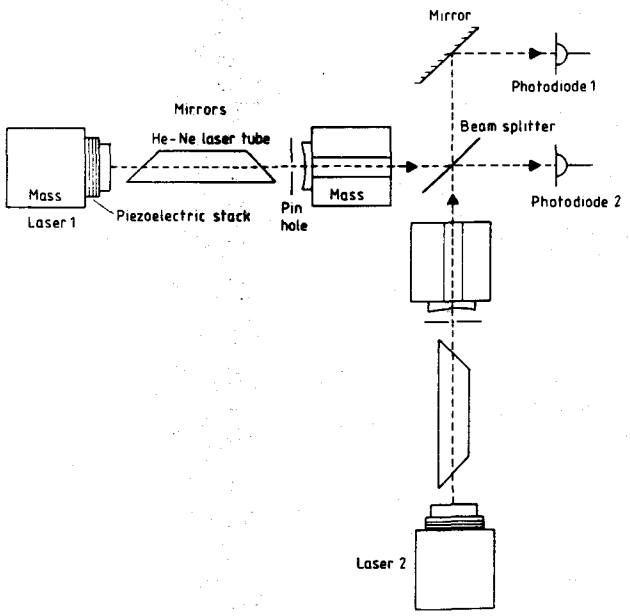

Figure 1. Optical layout of the active-cavity laser interferometer.

0022-3735/86/030182 + 07 $02.50

The two cavities are of slightly different length so that their axial mode spacings are 780 and 820 MHz, respectively. This difference in axial mode spacing is needed in order to make it possible to distinguish between the two lasers for stabilisation purposes. Since the gain bandwidth of the He–Ne mixture at 632.8 nm is about 1.5 GHz, asymmetric tuning allows the lasers to operate with only two longitudinal modes. Pinholes placed next to the output mirrors eliminate all but the lowest transverse mode. The laser cavities have a quality factor of $\sim 3 \times 10^8$.

Each laser tube is housed within a $12 \times 12 \times 18$ cm^3 aluminium central block, having the lowest vibrational mode at 8.5 kHz. The mirrors are rigidly mounted on cylindrical stainless steel test masses 10 cm long and 10 cm in diameter. The lowest vibrational mode of the masses is at 17.2 kHz and has a quality factor of about 300. One end of each mass is attached to the central block by two steel rods in a V configuration (see figure 2). The other end of the mass is attached by two thin wires to a pair of screws which allow alignment of the mass and thus of the corresponding mirror. The resonant frequency of this suspension is 25 Hz and is determined by the rods, which act as springs. The quality factor of the suspension is better than 320. In both lasers, the plane mirror is mounted on a stack of piezoelectric ceramics for cavity length tuning.

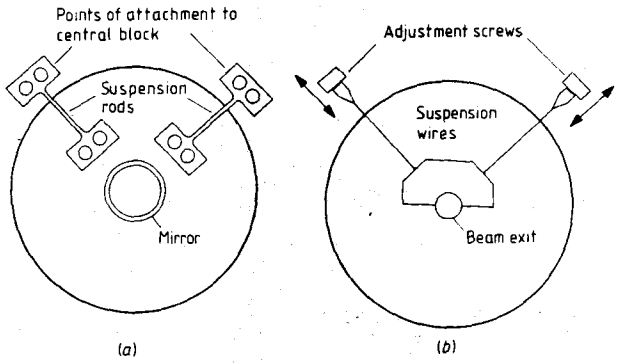

Figure 2. Test mass suspension arrangement.

The two laser assemblies together with the beam splitter and an additional deflection mirror are mounted on a $65 \times 65 \times 5$ cm^3 aluminium platform, which completes the compact and sturdy structure of the GR antenna.

2.2. Seismic and acoustic isolation

The entire detector assembly (see figure 3) is set up on a two-ton optical table placed on air mounts. The antenna platform is suspended from four steel wires, which are connected at their upper ends to isolation stacks consisting of alternating layers of steel and silicone rubber. Further isolation is provided by the test masses themselves being suspended as pendulums, as described in the previous section.

Due to the way they are suspended, the masses can, to a good approximation, only move axially. Axial noise excitation is transmitted to the masses mainly through the upper ends of the suspension rods, which are attached to the central block housing the laser tube. At frequencies in the kilohertz range, which are far above the pendulum frequency of the masses (25 Hz), this is a weak coupling and seismic noise undergoes strong attenuation before reaching the masses. On the other hand, frequencies around or below 25 Hz are far below the lowest vibrational mode of the central block (8.5 kHz), which thus behaves as a rigid body. Therefore, the upper attachment points of the suspension rods for a given pair of masses will experience no differential movement, i.e. there will be no change in mass

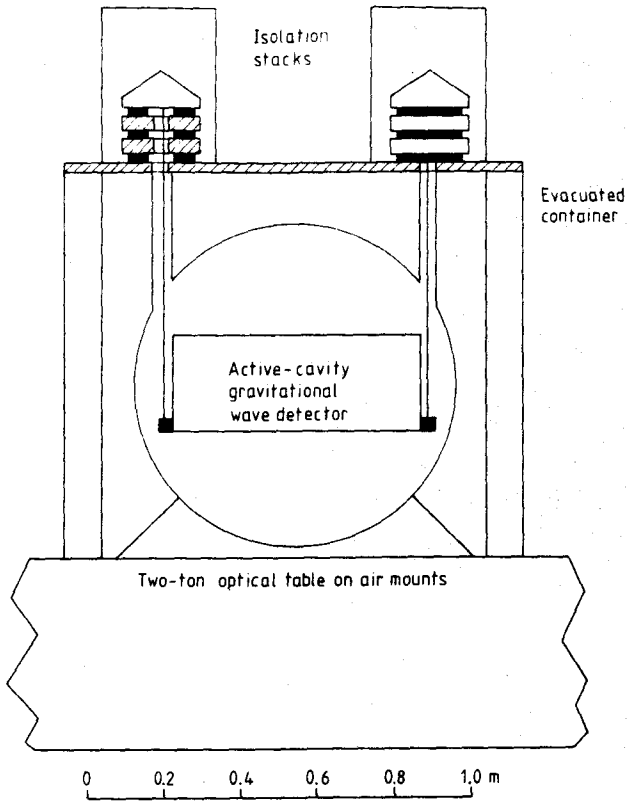

Figure 3. Isolation system of the GR detector.

spacing. This common mode noise rejection to first order substantially increases the efficiency of the seismic isolation at low frequencies.

Acoustic isolation is provided by maintaining the antenna and the isolation stacks within an evacuated enclosure.

Our open-cavity lasers tend to become misaligned during evacuation because of the difference between the refraction indices of air and vacuum ($n - 1 = 2.8 \times 10^{-4}$ for air at room temperature and atmospheric pressure). This is avoided by aligning the lasers in helium at atmospheric pressure ($n_{He} - 1 = 3 \times 10^{-5}$) prior to their transfer to the vacuum vessel.

2.3. Laser stabilisation and signal extraction

A block diagram of the electronics used to stabilise the lasers and measure the beat frequency is shown in figure 4.

Stabilisation of Laser 1 is taken care of by the upper loop. As explained above, the laser is operated with two longitudinal modes, spaced by approximately 820 MHz. As the modes are tuned across the gain curve, their spacing changes markedly (McFarlane 1964), which is used to derive the error signal (Weksler *et al* 1980b). For our particular lasers, the mode spacing changes by 360 kHz for a change in cavity length of $\frac{1}{4}\lambda$.

The difference of 40 MHz in axial mode spacing between the two lasers, mentioned in § 2.1, as well as the narrow bandwidth of the FM demodulator (0.5 MHz), allow us to apply the stabilisation procedure to the appropriate laser, although two pairs of axial modes (one from each laser) are present in the light beam reaching Photodiode 1. The resulting frequency drift rate for the stabilised laser is typically 1 MHz/hour.

The 20 MHz beat note between two selected modes, one from each laser, is obtained at the output of Photodiode 2. This photodector is loaded by a parallel RLC circuit with a resonant frequency of 20 MHz and a bandwidth of 3 MHz. The signal is amplified, split and directed toward the low-noise FM demodulator and the feedback path which stabilises the 20 MHz beat frequency between the two lasers.

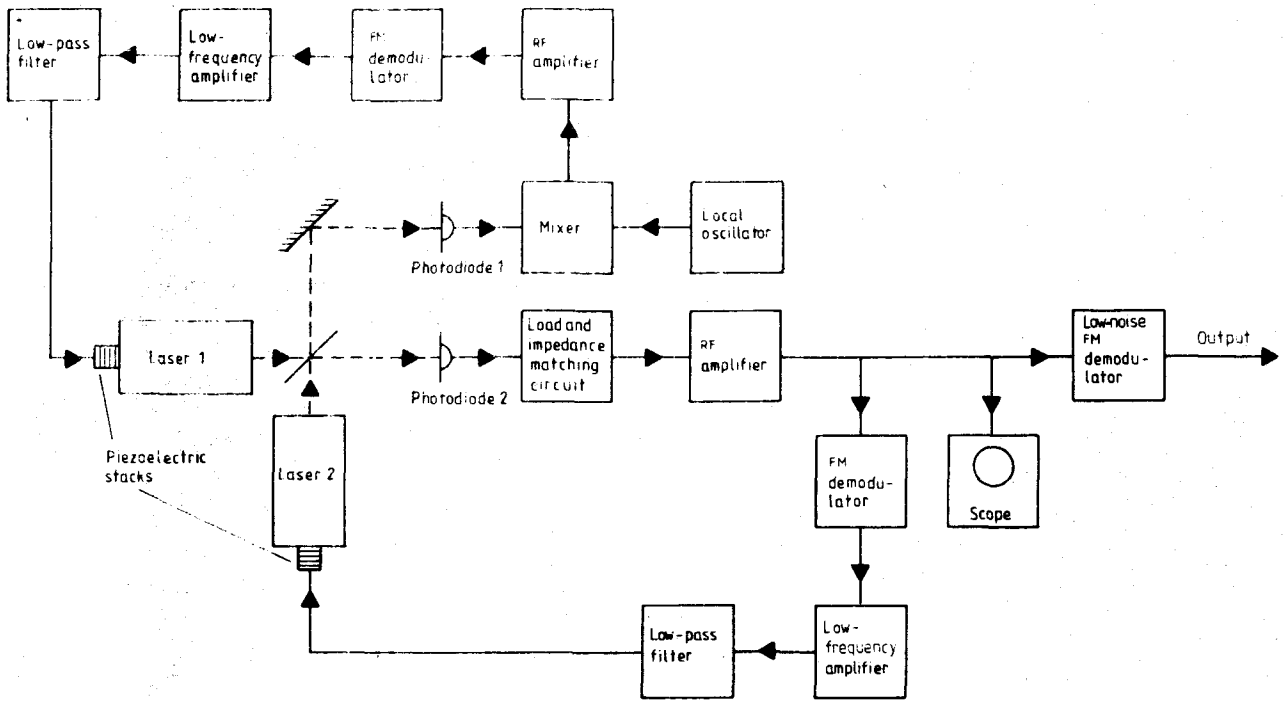

Figure 4. Block diagram of the electronics.

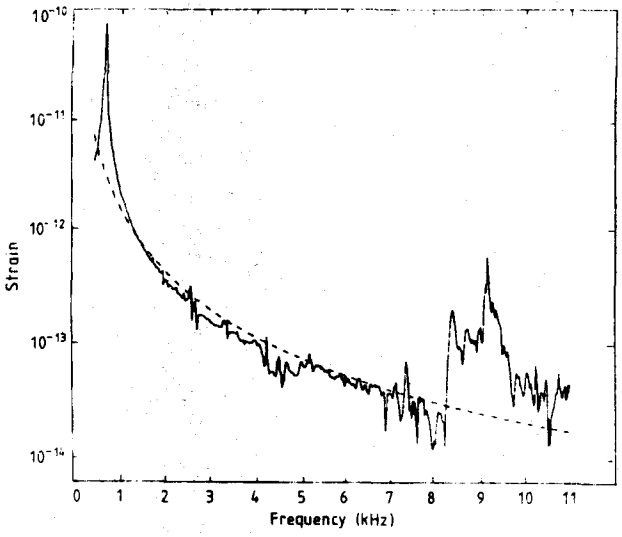

Figure 5. Detector calibration: FM demodulator output, translated to strain, against frequency of driving voltage. Full curve, measured output; broken curve, calculated output.

The low-noise FM demodulator monitoring small changes of the laser frequency is of the time delay type (Tykulsky 1966) and operates linearly over a bandwidth of 200 kHz.

It is stressed that the beat frequency stability requirement, which is set by the bandwidth over which the low-noise FM demodulator is linear, is mild and easily complied with. Much more stringent stability requirements apply to passive-cavity systems, where the beam of an external laser has to be passed through the very narrow bandwidth of high-quality cavities.

2.4. Antenna calibration

Calibration has been performed by electrostatically driving one of the suspended masses. To this purpose, an AC voltage of known amplitude was applied between the mass and two brass plates, attached to the central block in positions facing the mass. The resulting change in beat frequency was measured. A comparison between the calculated and measured response is presented in figure 5. The sharp peak at 740 Hz is an artifact due to the combination of the mechanical response of the mass with the transfer function of the servo-system that stabilises the 20 MHz beat frequency. Between 1 and 8 kHz the calculated strain agrees well with the measured one (see figure 5). Thus, within this band, the laser beat frequency stabilisation is no longer effective and the response of the mass is as required. The broad structure above 8 kHz consists of overlapping vibrational modes of the central block, which are directly excited by the calibration procedure.

3. Noise analysis

Noise enters the system at various points. To assess their relative importance, the noise contributions will be translated into equivalent fluctuations in laser cavity length, by multiplication with the appropriate coefficients.

Due to the efficiency of the isolation system, seismic and acoustic noise are currently well below the intrinsic noise of the sensor. Operating the laser tubes according to the instructions of the manufacturer resulted in no detectable plasma noise. The relevant noise sources affecting the displacement sensor and the electronics are discussed below.

3.1. Laser spontaneous emission noise

The intrinsic noise limiting the performance of the active-cavity GR detector consists of laser frequency fluctuations due to spontaneous emission. Their spectral density is (Yariv and Caton 1974)

$$\delta\omega^2(f)=\frac{\hbar\omega^3}{Q^2P}\,\frac{N_2}{[N_2-N_1(g_2/g_1)]} \qquad (2)$$

where f, Q, P, N_1, N_2, g_1 and g_2 are the frequency of the fluctuations, the quality factor of the cold laser resonator, the power lost by the stored laser field, the lower and upper laser level occupation numbers and the level multiplicities, respectively. For low-power operation, the lower laser level occupation is negligible and $N_2/[N_2-N_1(g_2/g_1)]=1$. For high-power lasers the losses are almost entirely due to the output

coupler transparency. Then, P is the output power of the laser. However, for our low-power lasers this is not the case and it is found that $P = 1.7P_{out}$.

Since a relative change $\Delta L/L$ in laser cavity length (where L is the optical path length of the resonator) causes an equal relative change $\Delta\omega/\omega$ in laser frequency, the frequency fluctuations of equation (2) are converted to laser length fluctuations $\delta x_1^2(f)$ by multiplication with L^2/ω^2. For the actual parameters of our lasers (see § 2), equation (2) yields

$$\delta x_1^2(f) = \frac{7.8 \times 10^{-31}}{P_{out}} \text{ cm}^2 \text{ Hz}^{-1} \tag{3}$$

where P_{out} is expressed in milliwatts. For a typical output power of 0.1 mW $\delta x_1(f) = 2.8 \times 10^{-15}$ cm Hz$^{-1/2}$, which shows that, even with low-power lasers, the active-cavity detector is capable of a displacement sensitivity as high as that of the large passive interferometers.

3.2. Thermal noise

A damped oscillator is subject to a noise driving force of spectral density $4kTM\Omega_0/Q_{osc}$, where k is the Boltzmann constant, T the absolute temperature, M the mass, $\Omega_0 = 2\pi f_0$ (f_0 being the eigenfrequency) and Q_{osc} the quality factor of the oscillator (Whalen 1971).

In the kilohertz band, which is far above the 25 Hz pendulum frequency of the mass suspensions, the fluctuations in mass position induced by the noise force have spectral density:

$$\delta x_2^2(f) = \frac{4kT\Omega_0}{MQ\Omega^4} \tag{4}$$

Substituting for our system parameters yields

$$\delta x_2^2(f) = \frac{8.7 \times 10^{-21}}{f^4} \text{ cm}^2 \text{ Hz}^{-1} \tag{5}$$

where f is the frequency of the fluctuations in hertz.

Thermal compressive forces lead to fluctuations in mass length. Below the first eigenmode of the masses, the resulting fluctuations in mirror position are of spectral density:

$$\delta x_3^2(f) = \frac{8kT}{MQ\Omega_0^3}. \tag{6}$$

For the actual values of the parameters of our detector, this yields

$$\delta x_3^2(f) = 1.46 \times 10^{-34} \text{ cm}^2 \text{ Hz}^{-1}. \tag{7}$$

3.3. Gas pressure fluctuations within the laser tube

Pressure fluctuations in the He–Ne mixture propagate as sound waves through the gas and result in fluctuations of the laser cavity optical length. A change Δp in gas pressure causes a change in gas refraction index of $\Delta n = (n_0 - 1)\Delta p/p_0$, which in turn modifies the He–Ne column optical path length by an amount $\Delta L = L_t(n_0 - 1)\Delta p/p_0$, where L_t is the length of the gas column ($L_t = 15$ cm for our laser tubes).

At the kHz frequencies of interest the wavelength of the sound waves is comparable with L_t. We will assume for simplicity that the pressure fluctuations affect the entire gas column simultaneously. We also assume that the gas is in thermal equilibrium, so that the spectral density of pressure fluctuations is (Callen and Welton 1951)

$$\delta p^2(f) = 4\pi \frac{\rho kT}{c_s} f^2 \tag{8}$$

where ρ is the density of the gas and c_s the velocity of sound. Accordingly, the spectral density of optical path length fluctuations is

$$\delta x_4^2(f) = 4\pi \frac{L_t^2(n_0 - 1)^2}{p_0^2 c_s} \rho kTf^{-2}. \tag{9}$$

To make things specific, a pressure of 4 Torr, a He:Ne pressure ratio of 5:1 and a gas temperature of 300 K are assumed, yielding, after substitution into equation (9),

$$\delta x_4^2(f) = 3 \times 10^{-42} f^{-2} \text{ cm}^2 \text{Hz}^{-1}. \tag{10}$$

3.4. Electronics and shot noise

The electronics noise consists mainly of photodiode noise and of Johnson noise generated at the photodiode load circuit. At resonance, the parallel RLC load circuit behaves as a resistor of 3.3 kΩ resistance. At room temperature, the Johnson noise current flowing through the resistor has a spectral density $\delta i_n^2(f) = 4kT/R = 5 \times 10^{-24}$ A^2 Hz^{-1}. Noise generated at the photodiode (FND-100 of EG&G-PAR) has a spectral density of 3.24×10^{-26} A^2 Hz^{-1} and can be neglected. The equivalent fluctuations in laser length are

$$\delta x_5^2(f) = 7.25 \times 10^{-51} \frac{f^2}{i_{pd}^2} \text{ cm}^2 \text{ Hz}^{-1} \tag{11}$$

where i_{pd} is expressed in amperes.

The noise due to the statistical photodetection process follows a Poisson distribution. The spectral density of photodetected current fluctuations (shot noise) is $2ei_{pd}$ (van der Ziel 1971), where e is the electron charge. The corresponding laser length fluctuations are

$$\delta x_6^2(f) = \frac{2L^2 e\Omega^2}{\omega^2 i_{pd}} \tag{12}$$

which, for the actual parameters of our detector, becomes

$$\delta x_6^2(f) = 4.6 \times 10^{-46} \frac{f^2}{i_{pd}} \text{ cm}^2 \text{ Hz}^{-1}. \tag{13}$$

4. System performance

4.1. Expected detector sensitivity

Summing up all the noise contributions yields the spectral density of noise equivalent displacements:

$$\delta x^2(f) = \sum_j N_j \delta x_j^2(f) \tag{14}$$

where N_j is the multiplicity of the noise source j. For instance, the thermal noise term $\delta x_2^2(f)$ given by equation (5), related to the mass suspension, has to be multiplied by four, because there are four masses. The spectral density of the lowest detectable strain then is

$$\delta s^2(f) = \frac{\delta x^2(f)}{4L_M^2} \tag{15}$$

where the factor four in the denominator accounts for the coherent addition of the signals in the two antenna arms and L_M is the distance between the centres of the two masses in one arm.

Although the two lasers are of similar construction, differences in laser tube quality led to different output powers, namely of 180 and 75 μW, respectively. Therefore, there are two distinct terms $\delta x_1^2(f)$ in equation (14), one for each value of the output power.

The beams are extracted from the vacuum vessel through an uncoated tilted window, therefore the optical power reaching the photodetector is slightly less than half the combined power of the two lasers. Accordingly, the appropriate value of the photocurrent entering equations (11) and (13) is 51 μA.

A numerical evaluation of equation (15) is given in figure 6. Also shown are the individual contributions of each noise source. Above 200 Hz, only laser FM noise due to spontaneous emission is expected to contribute significantly to system noise and the expected lowest detectable strain is

$$\delta s_{calc}(f) = 6.6 \times 10^{-17} \text{ Hz}^{-1/2}. \tag{16}$$

coupler transparency. Then, P is the output power of the laser. However, for our low-power lasers this is not the case and it is found that $P = 1.7P_{out}$.

Since a relative change $\Delta L/L$ in laser cavity length (where L is the optical path length of the resonator) causes an equal relative change $\Delta\omega/\omega$ in laser frequency, the frequency fluctuations of equation (2) are converted to laser length fluctuations $\delta x_1^2(f)$ by multiplication with L^2/ω^2. For the actual parameters of our lasers (see § 2), equation (2) yields

$$\delta x_1^2(f) = \frac{7.8 \times 10^{-31}}{P_{out}} \text{ cm}^2 \text{ Hz}^{-1} \tag{3}$$

where P_{out} is expressed in milliwatts. For a typical output power of 0.1 mW $\delta x_1(f) = 2.8 \times 10^{-15}$ cm Hz$^{-1/2}$, which shows that, even with low-power lasers, the active-cavity detector is capable of a displacement sensitivity as high as that of the large passive interferometers.

3.2. Thermal noise

A damped oscillator is subject to a noise driving force of spectral density $4kTM\Omega_0/Q_{osc}$, where k is the Boltzmann constant, T the absolute temperature, M the mass, $\Omega_0 = 2\pi f_0$ (f_0 being the eigenfrequency) and Q_{osc} the quality factor of the oscillator (Whalen 1971).

In the kilohertz band, which is far above the 25 Hz pendulum frequency of the mass suspensions, the fluctuations in mass position induced by the noise force have spectral density:

$$\delta x_2^2(f) = \frac{4kT\Omega_0}{MQ\Omega^4} \tag{4}$$

Substituting for our system parameters yields

$$\delta x_2^2(f) = \frac{8.7 \times 10^{-21}}{f^4} \text{ cm}^2 \text{ Hz}^{-1} \tag{5}$$

where f is the frequency of the fluctuations in hertz.

Thermal compressive forces lead to fluctuations in mass length. Below the first eigenmode of the masses, the resulting fluctuations in mirror position are of spectral density:

$$\delta x_3^2(f) = \frac{8kT}{MQ\Omega_0^3}. \tag{6}$$

For the actual values of the parameters of our detector, this yields

$$\delta x_3^2(f) = 1.46 \times 10^{-34} \text{ cm}^2 \text{ Hz}^{-1}. \tag{7}$$

3.3. Gas pressure fluctuations within the laser tube

Pressure fluctuations in the He–Ne mixture propagate as sound waves through the gas and result in fluctuations of the laser cavity optical length. A change Δp in gas pressure causes a change in gas refraction index of $\Delta n = (n_0 - 1)\Delta p/p_0$, which in turn modifies the He–Ne column optical path length by an amount $\Delta L = L_t(n_0 - 1)\Delta p/p_0$, where L_t is the length of the gas column ($L_t = 15$ cm for our laser tubes).

At the kHz frequencies of interest the wavelength of the sound waves is comparable with L_t. We will assume for simplicity that the pressure fluctuations affect the entire gas column simultaneously. We also assume that the gas is in thermal equilibrium, so that the spectral density of pressure fluctuations is (Callen and Welton 1951)

$$\delta p^2(f) = 4\pi \frac{\rho kT}{c_s} f^2 \tag{8}$$

where ρ is the density of the gas and c_s the velocity of sound. Accordingly, the spectral density of optical path length fluctuations is

$$\delta x_4^2(f) = 4\pi \frac{L_t^2(n_0 - 1)^2}{p_0^2 c_s} \rho kTf^{-2}. \tag{9}$$

To make things specific, a pressure of 4 Torr, a He:Ne pressure ratio of 5:1 and a gas temperature of 300 K are assumed, yielding, after substitution into equation (9),

$$\delta x_4^2(f) = 3 \times 10^{-42} f^{-2} \text{ cm}^2 \text{Hz}^{-1}. \tag{10}$$

3.4. Electronics and shot noise

The electronics noise consists mainly of photodiode noise and of Johnson noise generated at the photodiode load circuit. At resonance, the parallel RLC load circuit behaves as a resistor of 3.3 kΩ resistance. At room temperature, the Johnson noise current flowing through the resistor has a spectral density $\delta i_n^2(f) = 4kT/R = 5 \times 10^{-24}$ A^2 Hz^{-1}. Noise generated at the photodiode (FND-100 of EG&G-PAR) has a spectral density of 3.24×10^{-26} A^2 Hz^{-1} and can be neglected. The equivalent fluctuations in laser length are

$$\delta x_5^2(f) = 7.25 \times 10^{-51} \frac{f^2}{i_{pd}^2} \text{ cm}^2 \text{ Hz}^{-1} \tag{11}$$

where i_{pd} is expressed in amperes.

The noise due to the statistical photodetection process follows a Poisson distribution. The spectral density of photodetected current fluctuations (shot noise) is $2ei_{pd}$ (van der Ziel 1971), where e is the electron charge. The corresponding laser length fluctuations are

$$\delta x_6^2(f) = \frac{2L^2 e\Omega^2}{\omega^2 i_{pd}} \tag{12}$$

which, for the actual parameters of our detector, becomes

$$\delta x_6^2(f) = 4.6 \times 10^{-46} \frac{f^2}{i_{pd}} \text{ cm}^2 \text{ Hz}^{-1}. \tag{13}$$

4. System performance

4.1. Expected detector sensitivity

Summing up all the noise contributions yields the spectral density of noise equivalent displacements:

$$\delta x^2(f) = \sum_j N_j \delta x_j^2(f) \tag{14}$$

where N_j is the multiplicity of the noise source j. For instance, the thermal noise term $\delta x_2^2(f)$ given by equation (5), related to the mass suspension, has to be multiplied by four, because there are four masses. The spectral density of the lowest detectable strain then is

$$\delta s^2(f) = \frac{\delta x^2(f)}{4L_M^2} \tag{15}$$

where the factor four in the denominator accounts for the coherent addition of the signals in the two antenna arms and L_M is the distance between the centres of the two masses in one arm.

Although the two lasers are of similar construction, differences in laser tube quality led to different output powers, namely of 180 and 75 μW, respectively. Therefore, there are two distinct terms $\delta x_1^2(f)$ in equation (14), one for each value of the output power.

The beams are extracted from the vacuum vessel through an uncoated tilted window, therefore the optical power reaching the photodetector is slightly less than half the combined power of the two lasers. Accordingly, the appropriate value of the photocurrent entering equations (11) and (13) is 51 μA.

A numerical evaluation of equation (15) is given in figure 6. Also shown are the individual contributions of each noise source. Above 200 Hz, only laser FM noise due to spontaneous emission is expected to contribute significantly to system noise and the expected lowest detectable strain is

$$\delta s_{calc}(f) = 6.6 \times 10^{-17} \text{ Hz}^{-1/2}. \tag{16}$$

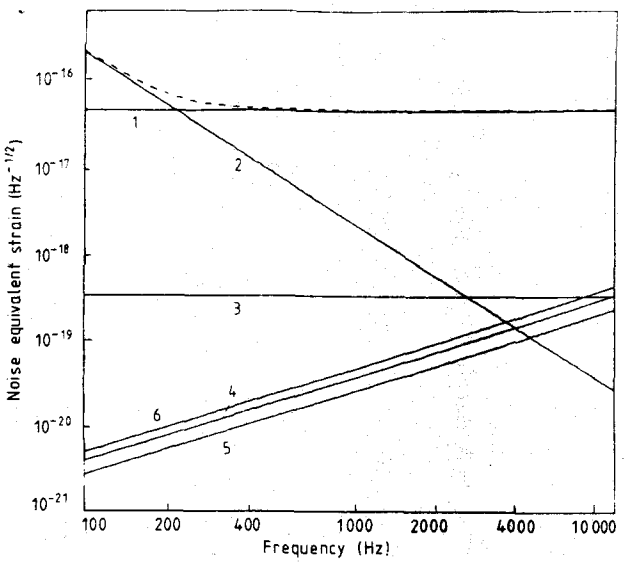

Figure 6. Spectral density of strain equivalent to various noise contributions: 1, laser spontaneous emission noise; 2, thermal noise in mass suspensions; 3, thermal noise in lowest vibrational mode of masses; 4, noise due to gas pressure fluctuations in the laser tubes; 5, thermal noise in photodiode load resistor; 6, shot noise. The broken curve is the sum of all noise contributions.

4.2. *Energy flux of a detectable* GR *event*

The minimum energy flux necessary to detect a GR event is evaluated as follows (Weksler 1980). The relation between the dimensionless gravitational wave (GW) amplitude $h(t)$ and the energy flux per unit time $W(t)$ is (Press and Thorne 1972)

$$W(t)=\dot{h}^2(t)\frac{L_0}{16\pi c^2} \tag{17}$$

where $L_0=3.6\times10^{52}\ \mathrm{J\,s^{-1}}$. The total energy flux E is obtained by integrating $W(t)$ over time. Using Parseval's theorem yields

$$E=\frac{L_0}{32\pi^2c^2}\int|H(\Omega)|^2\Omega^2\mathrm{d}\Omega \tag{18}$$

where $H(\Omega)$ is the Fourier transform of $h(t)$.

If an optimally matched filter and white noise are assumed, a signal-to-noise ratio equal to one (limiting detection condition) is obtained if (Whalen 1971)

$$\frac{1}{2\pi}\int|H(\Omega)|^2\mathrm{d}\Omega=\frac{\delta H_n^2}{2} \tag{19}$$

where δH_n^2 is the noise equivalent spectral density of the GW amplitude.

If knowledge about the shape of $H(\Omega)$ is available, its magnitude can be evaluated by use of equation (19). The result is then used with equation (18) to calculate the energy flux of a barely detectable GR event.

The spectrum of energy radiated as GW has been evaluated for various cosmic events (see, e.g., Kojima and Nakamura 1983 and references quoted therein). For example, the energy spectrum radiated by a particle falling into a black hole is a monotonically increasing function of frequency until, at some cut-off frequency (typically a few kilohertz for a black hole of ten solar masses), a sharp decrease occurs.

To estimate the order of magnitude of the lowest detectable energy flux, this behaviour may be crudely approximated by some power of Ω, with a cut-off at Ω_{max}. The simplest case is

$$H(\Omega)=\begin{cases}K & \text{for } \Omega<\Omega_{max}\\ 0 & \text{for } \Omega>\Omega_{max}\end{cases} \tag{20}$$

(K is a constant) which, according to equation (18), leads to a quadratic behaviour of the radiated energy spectrum.

4.3. *Measured detector sensitivity*

Detector noise is measured at the output of the low-noise FM demodulator. The observed noise level, converted to strain, is shown in figure 7. In a band extending from 2 kHz to more than 10 kHz, the noise spectrum is practically flat at about $10^{-16}\ \mathrm{Hz^{-1/2}}$, very close to the expected noise level given by equation (16). The feasibility of operating a very-high-sensitivity active-cavity interferometer at the spontaneous emission noise limit is thereby experimentally demonstrated.

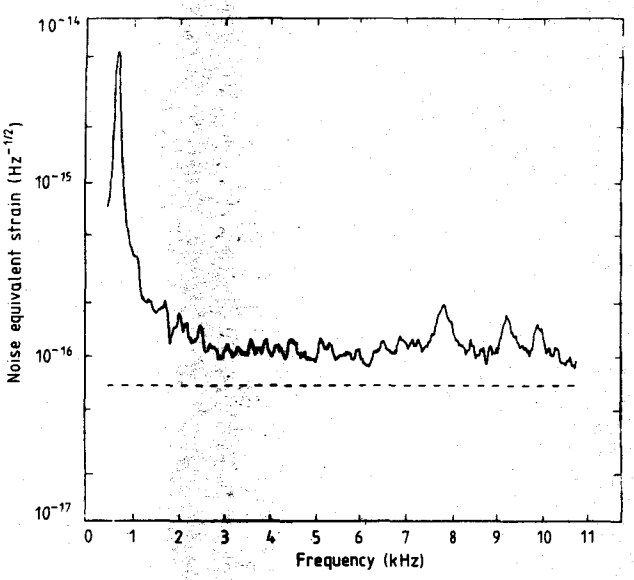

Figure 7. Measured noise spectrum. The broken line is the calculated spontaneous emission noise.

Over the bandwidth of ~10 kHz where the noise spectrum is flat, optimum filtering is easily achieved. For example, in the case of a signal with a flat spectrum, the lower limit on detectable strain that corresponds to our present noise level is $\sim 10^{-18}\ \mathrm{Hz^{-1}}$, according to equation (19).

The strain equivalent to the present noise level is roughly equal to that reported by Forward (1978) and higher by about two orders of magnitude than that achieved recently with the 30 m Michelson interferometer of the Max Plank Institute for Quantum Optics at Garching, Germany (Schilling *et al* 1984). However, the noise spectrum of our detector is flat over a wider band than that of the Garching detector, due to the more compact mechanical structure of the essential components, resulting in the absence of unwanted resonances.

The noise equivalent displacement for our detector is $3\times10^{-15}\ \mathrm{cm\,Hz^{-1/2}}$. In the kilohertz range, this is second only to that of the Garching group, $\sim10^{-15}\ \mathrm{cm\,Hz^{-1/2}}$. It should be added that a displacement noise of approximately $10^{-15}\ \mathrm{cm\,Hz^{-1/2}}$ has also been demonstrated at 1 MHz, using superconducting microwave resonators (Reece *et al* 1984).

The measured noise level is equivalent to fluctuations of $0.15\ \mathrm{Hz\,Hz^{-1/2}}$ in the 20 MHz beat frequency, which contains the FM noise of both laser beams. This is the lowest level of FM noise that has been demonstrated with a free-running laser at such low frequencies. A similar FM noise level has been measured above 100 kHz with a free-running He–Ne laser (Zaitsev and Stepanov 1967). Using the measured noise level and following the steps outlined in § 4.2, it is estimated

that the minimum detectable energy flux of a GR event is 5.2×10^6 J cm^{-2} for a cut-off frequency of 5 kHz.

5. Discussion: possible improvements in detector sensitivity

We have shown in § 4.3 that the present limit on performance of our detector is set by laser frequency fluctuations, which exceed other relevant noise contributions by more than two orders of magnitude in the kilohertz range (see figure 6). In order to identify ways to reduce laser frequency noise, its detailed dependence on laser parameters is described below.

The lowest detectable strain, determined by laser spontaneous emission noise, is obtained using equations (2), (14) and (15),

$$\delta s_1^2(f) = \frac{\hbar\omega L^2}{2Q^2 P L_M^2}. \tag{21}$$

The quality factor, Q, can be expressed in terms of the optical length, L, of the resonator, the vacuum wavelength, λ, of the laser field and the fractional loss per pass, a,

$$Q = 2\pi L/\lambda a \tag{22}$$

where $a = \alpha L_a - \ln(R_1 R_2)^{1/2}$, α is the loss coefficient of the active medium, L_a is the length of the active medium and R_1, R_2 are the reflectivities of the laser mirrors. Losses on intracavity optical surfaces (e.g. Brewster windows) are lumped into R_1, R_2.

For our low-gain, inhomogeneously broadened lasers, P, the power lost by the stored field, is (Rigrod 1963)

$$P = SI_s a[(g_0 L_a/a)^2 - 1] \sim SI_s (g_0 L_a)^2/a \tag{23}$$

where S, I_s and g_0 are the average cross-sectional area of the intracavity beam, the saturation parameter and the unsaturated gain coefficient, respectively. For the He–Ne amplifying medium α is negligible and therefore $a = -\ln(R_1 R_2)^{1/2}$. The laser output power is obtained by multiplying P by the ratio $T/2a$, where T is the transparency of the output mirror. Combining equations (21)–(23) yields

$$\delta s_1^2(f) = \frac{\hbar c\lambda a^3}{4\pi SI_s (g_0 L_a L_M)^2}. \tag{24}$$

Little can be done to improve the He–Ne laser tube performance. However, mirrors with 3×10^{-4} loss and 10^{-4} transparency are available commercially, for example from OCLI. Using such mirrors and using the measured loss of 0.1% on the Brewster windows, it should be possible to reduce the loss per pass by a factor of seven. This would reduce $\delta s_1(f)$ by a factor of only 18.

A more effective reduction in noise can be achieved by employing also a high-gain, low-loss amplifying medium. For instance, Nd:YAG operating at 1.064 μm seems well suited. For high-gain, homogeneously broadened lasers like the Nd:YAG ones, the power lost by the field is (Rigrod 1965) $SI_s g_0 L_a$. Therefore, using equations (21) and (22) yields

$$\delta s_1^2(f) = \frac{\hbar c\lambda a^2}{4\pi SI_s g_0 L_a L_M^2}. \tag{25}$$

Rods of Nd:YAG can be grown that have very low loss ($\alpha = 0.002$ cm^{-1}), high saturation parameter ($I_s \sim 2.5 \times 10^3$ W cm^{-2}) and high gain coefficient ($g_0 \sim 0.1$ cm^{-1}). For mirror losses as mentioned above, 0.5×10^{-3} losses on the rod end faces, $L_a = 1$ cm and $S = 10$ mm^2, equation (25) yields a lowest detectable strain of 10^{-19} Hz$^{-1/2}$.

A complication arises from the fact that Nd:YAG has a 120 GHz gain profile, which means that more than a hundred axial modes may lase simultaneously for a typical longitudinal mode spacing of ~ 1 GHz. However, a promising way to achieve stable single-mode operation of a Nd:YAG laser without using intracavity components (that inevitably have some insertion loss and thus lower the cavity Q) has been recently reported (Kane and Byer 1985). The extent to which thermal effects due to the high pumping level may generate excess noise and thus interfere with reaching the spontaneous emission noise limit with Nd:YAG lasers has still to be assessed experimentally.

Prospects for small-size active-cavity GR detectors to achieve strain sensitivities better than 10^{-19} Hz$^{-1/2}$ look encouraging. It should be remembered that the best quoted sensitivity to date, 5×10^{-19} Hz$^{-1/2}$, has been achieved within a narrow frequency range by using a 30 m shot-noise-limited multipass Michelson interferometer (Schilling *et al* 1984).

In view of the above evaluation, which shows that active-cavity detectors are potentially of the same sensitivity as passive ones, it is worth listing practical advantages of small-size active-cavity GR detectors.

- The small distance between the masses allows them to be attached to a rigid central block, which substantially improves seismic isolation at low frequencies by common-mode noise rejection.
- The mechanical structure of the detector is simple, sturdy and stable. As a consequence, a smooth mechanical frequency response is obtained, free of resonances within the frequency range of interest.
- The time spans involved in designing and manufacturing detector parts are short, speeding up detector development.
- A low-priced vacuum system easily covers the acoustical isolation needs of the detector.
- Only two servo-loops are needed in order to control the length of the resonators.
- Since each cavity generates its own field, there is no need to lock the frequency of the field to the eigenfrequency of a very-narrow-band (high-Q) resonator. The necessary degree of frequency stability is set by the bandwidth of the electronics used to process the beat frequency and by the need to stay within quiet areas of the gain curve. The resulting stability requirement is not very stringent.
- Finally, a large array of such units may be set up in order to obtain directivity as well as increased sensitivity.

6. Conclusions

A prototype GR detector with an active-cavity laser displacement sensor has been designed, built and tested. A rather flat noise spectrum has been measured above 2 kHz. It is equivalent to a lowest detectable strain of 10^{-16} Hz$^{-1/2}$ (corresponding to a change in spacing between the masses of 3×10^{-15} cm Hz$^{-1/2}$), and is close to the expected limit of 6.6×10^{-17} Hz$^{-1/2}$ set by laser frequency fluctuations due to spontaneous emission.

It has been shown that use of high-quality mirrors and a high-gain, low-loss amplifying medium (Nd:YAG) may lead to an improvement in sensitivity by three orders of magnitude, making the active-cavity detector a serious contender in the effort to detect gravitational radiation.

Small GR detectors benefit from a series of practical advantages, like short development time spans and low cost. The use of active cavities provides the additional bonus of mild frequency stability requirements. Thus, it becomes feasible to set up large arrays of active-cavity GR detectors which, in addition to improved sensitivity, will have the desirable feature of directivity.

Acknowledgments

We wish to thank Professor Arno Penzias for several stimulating discussions and useful suggestions. We are indebted to Maurice Algranati for his dedicated help with the electronics.

References

Bagayev S N, Chebotayev V P, Dychkov A S and Goldort V G 1981 On the possibility of using lasers as detectors of gravitational waves
Appl. Phys. **25** 161

Billing H, Maischberger K, Ruediger A, Schilling R, Schnupp L and Winkler W 1979 An argon laser interferometer for the detection of gravitational radiation
J. Phys. E: Sci. Instrum. **12** 1043

Callen H B and Welton T A 1951 Irreversibility and generalised noise
Phys. Rev. **83** 34

Drever R W P 1982 Interferometric detectors for gravitational radiation
Proc. NATO Advanced Study Institute on Gravitational Radiation, Les Houches 1982 (Amsterdam: North-Holland)

Forward R L 1978 Wideband laser interferometer gravitational radiation experiment
Phys. Rev. D **17** 379

Kane T J and Byer R L 1985 Monolithic, unidirectional single-mode Nd:YAG ring laser
Opt. Lett. **10** 65

Kojima Y and Nakamura T 1983 Gravitational radiation by a particle with nonzero orbital angular momentum falling into a Kerr black hole
Phys. Lett. **99A** 37

Linsay P, Saulson P and Weiss R 1983 A study of a long baseline gravitational wave antenna system
Report to the NSF

McFarlane R A 1964 Frequency pushing and frequency pulling in a He–He gas optical maser
Phys. Rev. **135** A543

Press W H and Thorne K S 1972 Gravitational-wave astronomy
Ann. Rev. Astron. Astrophys. **10** 335

Reece C E, Reiner P J and Melissinos A C 1984 Observation of 4×10^{-17} cm harmonic displacement using a 10 GHz superconducting parametric converter
Phys. Lett. **104A** 341

Rigrod W W 1963 Gain saturation and output powers of optical masers
J. Appl. Phys. **34** 2602

Rigrod W W 1965 Saturation effects in high gain lasers
J. Appl. Phys. **36** 2487

Schilling R, Schnupp L, Shoemaker D H, Winkler W, Maischberger K and Ruediger A 1984 Improved sensitivities in laser interferometers for the detection of gravitational waves
Max Planck Inst. for Quantum Optics Report MPQ 88

Tykulsky A 1966 Spectral measurements of oscillators
Proc. IEEE **54** 306

Weiss R 1972 Electromagnetically coupled broad band gravitational antenna
Q. Prog. Rep. Res. Lab. Electron. MIT **105**

Weksler M 1980 A sensitive laser sensor for a gravitational radiation detector
Thesis Weizmann Institute of Science

Weksler M, Vager Z and Neumann G 1980a Laser displacement sensor with application to gravitational wave detection
Appl. Opt. **19** 2717

Weksler M, Vager Z and Neumann G 1980b Measurement of a very high displacement sensitivity of the beat frequency in a He–Ne laser
IEEE J. Quantum Electron. **QE-16** 785

Whalen A D 1971 *Detection of Signals in Noise* (New York: Academic)

Winkler W 1983 Eine optische Verzoegerungsleitung fuer ein breitband Gravitationswellenexperiment
Max Planck Inst. for Quantum Optics Report MPQ 74

Yariv A and Caton W M 1974 Frequency, intensity and field fluctuations in laser oscillators
IEEE J. Quantum Electron. **QE-10** 509

Zaitsev Y N and Stepanov D P 1967 Gas laser frequency fluctuations
Sov. Phys.–JETP Lett. **6** 209

van der Ziel A 1971 *Noise* (Englewood Cliffs, NJ: Prentice Hall)